Sedimentary Geology 282 (2012) 336–346

Contents lists available at SciVerse ScienceDirect

Sedimentary Geology

journal homepage: www.elsevier.com/locate/sedgeo

High-resolution clay mineralogy as a proxy for orbital tuning: Example of the Hauterivian–Barremian transition in the Betic Cordillera (SE Spain)

Mathieu Moiroud [a,*], Mathieu Martinez [a], Jean-François Deconinck [a], Fabrice Monna [b], Pierre Pellenard [a], Laurent Riquier [a,c], Miguel Company [d]

[a] UMR CNRS 6282 Biogéosciences, Université de Bourgogne, 6Bd Gabriel, 21000 Dijon, France
[b] UMR CNRS 5594 ARTéHIS, Université de Bourgogne, 6Bd Gabriel, 21000 Dijon, France
[c] UMR CNRS 7193 ISTEP, Université Pierre et Marie Curie-Paris 6, 4, Place Jussieu, 75252 Paris Cedex 05, France
[d] Departamento de Estratigrafía y paleontología, Facultad de Ciencias de Granada, 18002 Granada, Spain

ARTICLE INFO

Article history:
Received 8 February 2012
Received in revised form 14 August 2012
Accepted 5 October 2012
Available online 17 October 2012

Editor: G.J. Weltje

Keywords:
Clay minerals
Cyclostratigraphy
Hauterivian
Barremian
Palaeoclimate
Faraoni Oceanic Anoxic Event

ABSTRACT

The response of clay mineral assemblages to potential orbital forcing is tested in Mesozoic hemipelagic marl–limestone rhythmites of the Río Argos section (Betic Cordillera, Southeastern Spain). Along the section, marls are pervasively enriched in kaolinite and illite, whereas limestones are enriched in smectite-rich illite/smectite mixed-layers, suggesting that marl–limestone alternations are produced by cyclic high-frequency fluctuations of continental runoff. Spectral analyses show that clay mineral assemblages evolve accordingly to precession, obliquity and eccentricity cycles. Durations of ammonite zones are assessed at 535 kyr for the Late Hauterivian *Pseudothurmannia ohmi* Zone and at 645 kyr and for the Early Barremian *Taveraidiscus hugii* Zone. These durations are in agreement with other cyclostratigraphic estimates but significantly differ from the Geologic Time Scale 2004 and 2008. Clay minerals display enhanced amplitude of the eccentricity cycles during the Faraoni Oceanic Anoxic Event due to enhanced continental weathering conditions prevailing at that time. Sedimentary expression of the 405-kyr eccentricity is disturbed by palaeoclimate changes during the Faraoni OAE, challenging the hypothesis of Cretaceous OAE triggered by eccentricity cycles. Although palaeoceanographic events (e.g. Faraoni OAE) may induce disturbances in the clay mineral record, this study demonstrates the potential of these minerals to be used as a proxy for orbital calibration in Mesozoic times.

© 2012 Elsevier B.V. All rights reserved.

1. Introduction

During the last decades, cyclostratigraphy has offered higher temporal resolution to improve the Geological Time Scale (GTS). The method has been successfully applied for the Neogene and progressively used for older sedimentary series (Lourens et al., 2004). As orbital calibration of the Cenozoic reaches its final stage with the characterisation of the Paleocene (Hilgen et al., 2010), other studies start to focus on the Cretaceous and the Jurassic in order to extend the time-stratigraphic framework to the Mesozoic (Boulila et al., 2010a,b; Husson et al., 2011). Since radiometric ages are scarce in the Early Cretaceous, cyclostratigraphy has become a major tool to improve the time frame accuracy (Herbert, 1992; Grippo et al., 2004; Gale et al., 2011). Hauterivian and Barremian stage time frames are currently based on indirect methods such as magnetostratigraphy (Ogg and Smith, 2004) and strontium-isotope stratigraphy (McArthur et al., 2007). Consequently, duration estimates of the *Pseudothurmannia ohmi* Zone (latest Hauterivian) vary from 1900 kyr (Gradstein et al., 2004) to 200 kyr (Ogg et al., 2008). Previous cyclostratigraphic studies provided duration estimates for the Hauterivian and Barremian stages but these studies were mostly based on precession cycle counting (Rio et al., 1989; Huang et al., 1993; Giraud, 1995; Fiet and Gorin, 2000). Recent developments in astrochronology recommend the use of the eccentricity cycles to estimate precise durations (Hinnov and Ogg, 2007). Hence, the use of time-series analyses performed on palaeoclimate proxies is required for a reliable identification of orbital cycles in the sedimentary record.

The development of astronomical solutions allowed period assessments of the Earth orbital cycles (Laskar et al., 2004). These cycles are widely used to establish durations, and to correlate and interpret sedimentary successions. Gravitational perturbations from the Sun, the Moon and other celestial bodies in the Solar System generate periodic movements of the Earth's axis, i.e. obliquity and precession, as well as orbital eccentricity (Milankovitch, 1941; Laskar et al., 2004). Due to chaotic interactions in the solar system, orbital periodicities change over geological time. Physical models postulate for a long, steady 405-kyr-eccentricity cycle (Laskar et al., 2004, 2011). This cycle is therefore preferred to provide accurate deposit durations (Meyers and Sageman, 2004; Huang et al., 2010; Voigt and Schönfeld, 2010).

* Corresponding author.
E-mail address: mathieu.moiroud@u-bourgogne.fr (M. Moiroud).

0037-0738/$ – see front matter © 2012 Elsevier B.V. All rights reserved.
http://dx.doi.org/10.1016/j.sedgeo.2012.10.004

Orbital fluctuations are the main causes of modifications in the Earth's insolation, which are amplified through complex feedback mechanisms in the climate system (Berger and Loutre, 2004; Strasser et al., 2006). Detrital supplies and sedimentation style can therefore be astroclimatically driven (Cotillon et al., 1980; Deconinck and Chamley, 1983; Mutterlose and Ruffell, 1999).

Special interest has been given to marl–limestone alternations, which are nowadays thought to result from cyclic fluctuations of marine and/or continental environments, affecting biological productivity, as well as the amount and nature of detrital particles, diluting the carbonate fraction (Darmedru, 1984; Sprenger and Ten Kate, 1993; Cotillon and Giraud, 1995; Foucault and Mélières, 2000; Voigt and Schönfeld, 2010). As clay mineral formation and sedimentation partly depend on climate (Chamley, 1989), marl–limestone alternations should theoretically record astronomical periods. Some studies have previously discussed the relation between precession cycles and clay mineral variations, but the influences of obliquity and eccentricity have yet to be precisely quantified (Cotillon et al., 1980; Mutterlose and Ruffell, 1999; Vanderaveroet et al., 1999; Foucault and Mélières, 2000).

The aim of this paper is to assess the ability of clay minerals to record astroclimate forcing in marl–limestone alternations, and to evaluate their potential to serve as proxies for orbital tuning. High-resolution mineralogical studies were therefore performed on a rhythmically bedded, hemipelagic succession, leading to more precise ammonite zone durations at the Hauterivian–Barremian transition. In addition, clay mineralogy response to oceanographic perturbations, such as the Faraoni Oceanic Anoxic Event (F-OAE), is examined.

2. Geological setting

2.1. The Subbetic Domain and the Río Argos section

The Subbetic Domain is located in southeastern Spain in the Betic Cordillera. During the Hauterivian–Barremian transition, this domain was situated on the southern palaeomargin of the Iberian plate at low latitudes between 20° and 30°N (Masse et al., 1993). From the Late Jurassic to the Early Cretaceous, it was a passive margin, with thick hemipelagic post-rift sedimentation smoothing the submarine relief (Martín-Algarra et al., 1992; Barbero and López-Garrido, 2006; Fig. 1).

The Río Argos succession, located near Caravaca de la Cruz (Murcia Province), is the most complete, well-preserved outcrop of marl–limestone alternations for the Lower Cretaceous. Slightly bioturbated, light grey to yellowish micritic calcareous beds alternate with darker marly interbeds (Hoedemaeker and Leereveld, 1995). Bed thickness fluctuates from one to several decimetres, while interbed thickness can occasionally reach one metre. There is no sedimentological evidence of hydrodynamic features, obvious sedimentary hiatuses in the section. Additionally, lime-mud export from Iberian carbonate ramps was likely limited, as any reworked shallow benthic fauna, sediments or turbidites were encountered. Alternations are mostly regarded as formed by fine particles of planktonic organisms, and clay minerals deposited by decantation in quiet, deep environments. In the Berriasian part of the section, marl–limestone alternations bundling have been attributed to orbital forcing (Sprenger and Ten Kate, 1993). This interpretation was extended to the Berriasian–Aptian throughout the Western Tethys (Hoedemaeker, 1998). Limestone beds contain nannofossils, including coccolithophorids and nannoconus tests. Macrofauna mainly consist in sparse belemnite guards and well-preserved ammonites, allowing detailed biostratigraphic zonation and accurate correlations of the sections (Company, 1987; Company et al., 1995, 2003; Hoedemaeker and Leereveld, 1995; Aguado et al., 2000). All these observations suggest a hemipelagic environment, with an estimated water depth of several hundreds of metres (Hoedemaeker and Leereveld, 1995).

The section studied, X.Ag-1 (Company et al., 2003), encompasses the *P. ohmi* and *Taveraidiscus hugii* ammonite zones at the Hauterivian–Barremian transition. The Faraoni Oceanic Anoxic Event (F-OAE) is recorded in the lowermost part of the *P. ohmi* zone (Fig. 3). This section, as a candidate for the Hauterivian–Barremian boundary GSSP (Gradstein et al., 2004; Ogg et al., 2008), contains all the official ammonite subzones, with no identifiable slumps or turbidites to disturb the sedimentary record (Hoedemaeker and Leereveld, 1995; Company et al., 2003).

2.2. Climate during the Hauterivian–Barremian transition

The Cretaceous has often been described as a warm equable "greenhouse" period (Barron, 1983; Hallam, 1985). However, more recent studies have reported the occurrence of cooler events during the Early Cretaceous before the thermal maximum of the Late Cenomanian-Early Turonian, which was followed by a cooling trend until the Maastrichtian (Price, 1999; van de Schootbrugge et al., 2000; Pucéat et al., 2003; McArthur et al., 2007). The Upper Hauterivian sediments recorded the F-OAE in the whole Western Tethyan domain (Baudin, 2005; Bodin et al., 2009), which corresponds to a slight positive

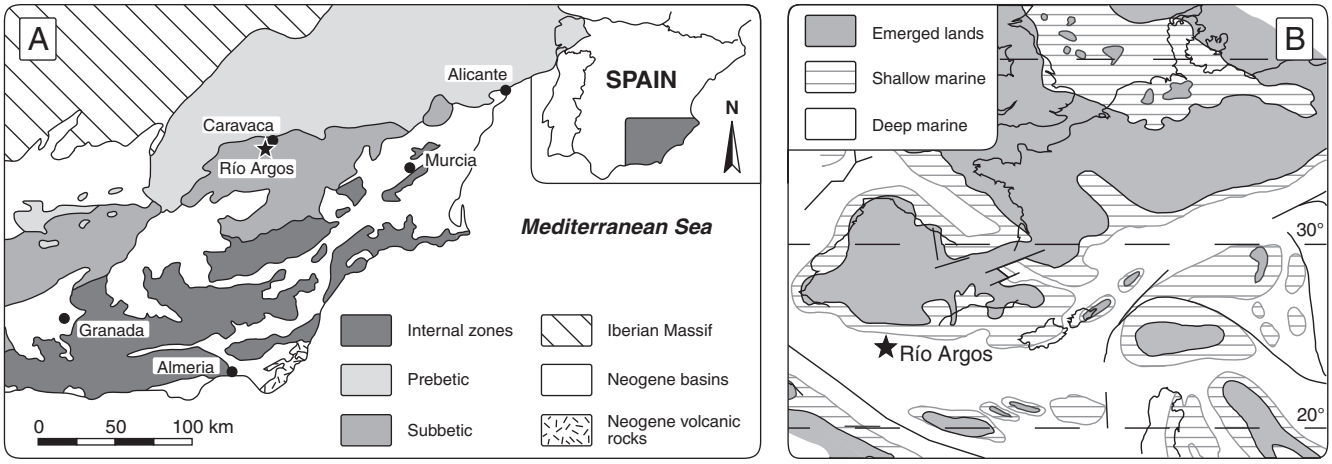

Fig. 1. (A) Simplified geological map of southeastern Spain showing the structural units of the Betic Cordillera, and location of the Río Argos section. (B) Palaeogeographic map of the Western Tethys for Hauterivian–Barremian times with location of the section.
(Modified from Baudin, 2005).

excursion of $\delta^{13}C$, interpreted as enhanced storage of organic carbon in marine environments following higher runoff under warmer and more humid conditions (Baudin, 2005; Godet et al., 2006; Bodin et al., 2009). Previous cyclostratigraphic studies have estimated the duration of this brief episode to be ca. 150 kyr (Baudin et al., 2006; Martinez et al., 2012).

In the Western Tethyan domain, clay mineral data from Hauterivian and Barremian sediments are available for the Sierra de Fontcalent section (Prebetic Zone) located close to Alicante (Rasplus et al., 1987). Illite is the most common mineral, in higher proportion to I/S mixed-layers; chlorite is relatively abundant, while kaolinite remains lower than 5%. Interestingly, illite increases from the Hauterivian to the Barremian. Data are also available in sections from the Vocontian Basin (SE France), notably on the Angles section (Deconinck, 1992; Godet et al., 2008). Compared to the Late Hauterivian, the Early Barremian interval is characterised by more illite and the common occurrence of kaolinite, suggesting more humid conditions with increasing runoff. The concomitant rise of $\delta^{13}C$ values was tentatively explained as the result of increased dissolved inorganic carbon input to the ocean (Godet et al., 2006).

3. Methods

3.1. X-ray diffraction and calcimetry

A total of 202 rock specimens were sampled along the 40.9 m of the X.Ag-1 section with a ~20 cm interval. Each specimen was cleaned, crushed, cleared of altered parts and macrofossils and then finely powdered, using a metal ring grinder.

Clay minerals were identified by X-ray diffraction (XRD) on oriented mounts of non-calcareous clay-sized particles (<2 μm), following the analytical procedure of Moore and Reynolds (1997). After removing carbonate using 0.2 N HCl, deflocculation of clays was completed by repeated washing with distilled water. Particles finer than 2 μm were concentrated by centrifugation. Diffractograms were obtained using a Bruker D4 Endeavor diffractometer with CuKα radiations, LynxEye detector and Ni filter, under 40 kV voltage and 25 mA intensity. The first XRD run was performed after air-drying, the second after ethyleneglycol solvation, and the third after heating at 490 °C for 2 h. The goniometer scanned from 2.5° to 28.5° for each run. Clay minerals were identified by the position of their main diffraction peaks on the three XRD runs, while semi-quantitative estimates were produced in relation to their area (Moore and Reynolds, 1997). Areas were determined on diffractograms of glycolated runs with MacDiff 4.2.5 software (Petschick, 2000). Beyond the evaluation of the clay minerals absolute proportions, the objective is to identify their relative fluctuations along the section. Peak area ratios were then considered for time-series analyses.

Calcimetry was performed on each powdered sample following the volumetric method employing a Bernard calcimeter (uncertainties below 5%; Lamas et al., 2005) to align $CaCO_3$ content with field observations and clay mineral assemblages.

3.2. Spectral analysis

Series were first resampled at 1 cm intervals using linear interpolation, and then detrended with a linear model (Weedon, 2003). Mineralogical data were transformed from stratigraphic to frequency domains using the Multi-Taper Method (MTM; Thomson, 1982, 1990) implemented in AnalySeries (Paillard et al., 1996). Three 2π tapers were used to ensure high frequency resolution while maintaining suitable confidence levels (2π-MTM). Peak significances were tested against a robust, first-order red-noise model – AR(1) – computed under the SSA-MTM Toolkit (Mann and Lees, 1996; Ghil et al., 2002).

3.3. Astrocycle identification and orbital calibration

Theoretical orbital periods for the Hauterivian are obtained from the astronomical solutions of Laskar et al. (2004). The classical frequency ratio comparison is used to link sedimentary to orbital frequencies (Huang et al., 1993; Boulila et al., 2008).

Due to the chaotic motion of the solar system and tidal dissipation effects, periods of precession and obliquity are not well constrained for geological times before ca. 40 Ma (Laskar et al., 2004). The long-term eccentricity (405 kyr) displays a stable period over Meso-Cenozoic times (Laskar et al., 2011); the series are therefore calibrated to this cycle for duration estimates (orbital tuning procedure). The short-term eccentricity (~100 kyr) is used if the long eccentricity is not identified on spectra. Gaussian band-pass filtering (AnalySeries) helps to identify eccentricity cycles. Eccentricity

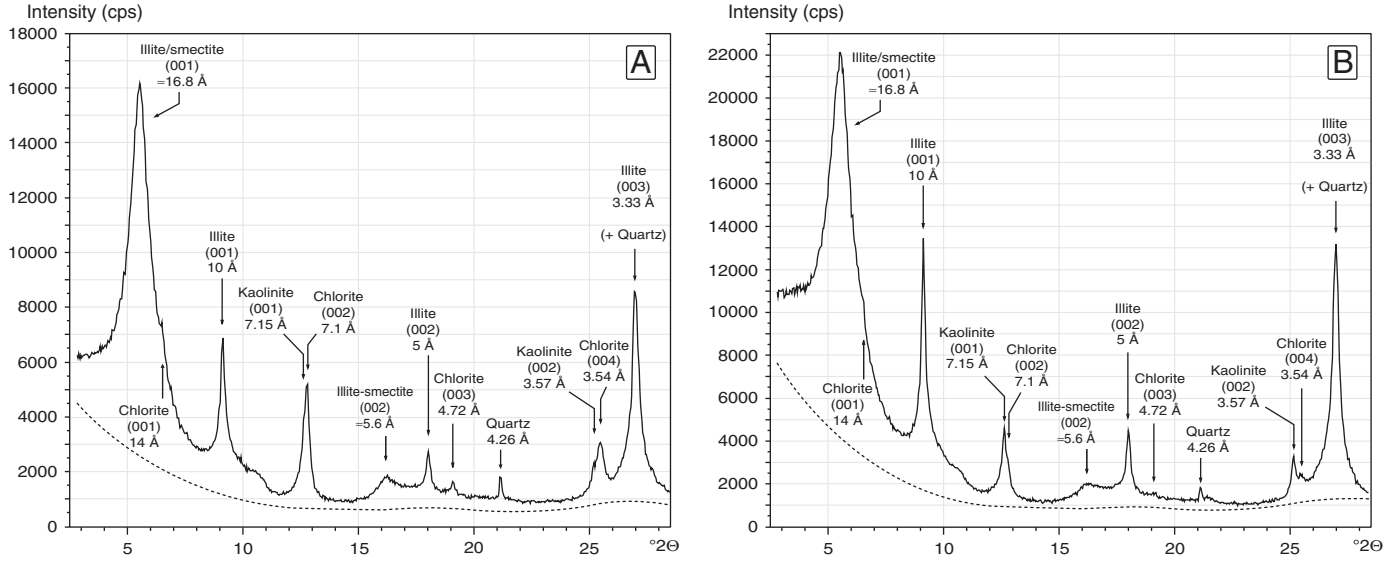

Fig. 2. Diffractograms of glycolated runs for (A) a limestone bed sample and (B) a marly interbed sample. Note the higher proportions of the (002) peak of kaolinite and (001) peak illite in marls (B) compared to limestone (A).

extrema are then used as tie-points to anchor the orbital tuning (LineAge function, AnalySeries), allowing estimates of durations.

4. Mineralogical results

Marl–limestone couplets are generally visible in the field because weathering tends to enhance lithological contrasts. Although average values of $CaCO_3$ are significantly lower in interbeds (58%) than in beds (76%), there is a fair amount of overlap in $CaCO_3$ content, which varies from 59% to 88% in beds and from 38% to 79% in interbeds (Fig. 4). As beds can be macroscopically compared to limestone and interbeds to marl in the field, despite fluctuating $CaCO_3$ contents, we use herein the terms "marl" and "limestone" in a descriptive sense (Munnecke et al., 2001). The clay mineral assemblages are relatively homogeneous and dominated by random I/S mixed-layers. The semi-quantification of these mixed-layers was complicated by the occurrence of quartz in the clay fraction, which prevents the common use of the (003)/(005) peaks; measurements on the (001) peak gave a proportion between 72% and 93% of the clay fraction (Figs. 2 and 3). The "saddle/(001) peak intensity ratio" or "saddle index" (Inoue et al., 1989), developed with an error margin of 10-15%, indicates that smectite layer content above 50% along the section, corresponding to smectite-rich I/S mixed-layers (*R0* I/S; Moore and Reynolds, 1997). The abundance of illite is comprised between 5 and 22%, while kaolinite and chlorite range from traces to 5 %. Illite content increases at the expense of I/S from the Hauterivian to the Barremian (Fig. 3), as on the Sierra de Foncalent section (Prebetic zone) and the Angles section (Vocontian Basin, SE France). Kaolinite abundance displays three depletion/enrichment cycles at intervals along the section: 0–14 m, 14–28 m and 28–41 m in height (Fig. 3). The F-OAE is characterised by greater fluctuations in chlorite and kaolinite content.

Three clay mineral ratios were also considered: the (002) diffraction peak of kaolinite (3.57 Å) on the (004) peak of chlorite (3.54 Å),

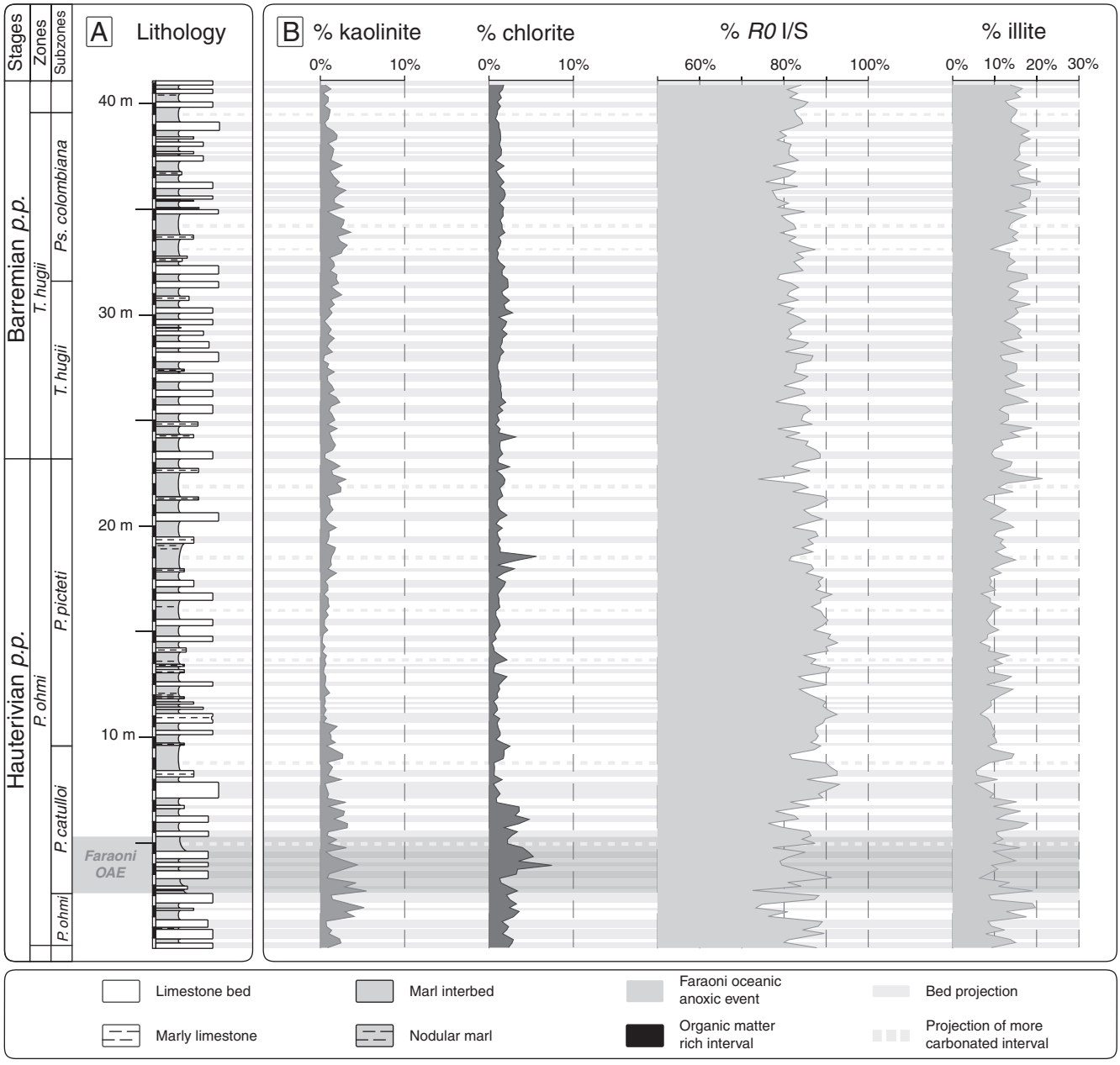

Fig. 3. Lithology and clay mineralogy of the X.Ag-1 section. Solid grey lines: limestone beds, dotted grey lines: non-indurated limestone bed inferred from the total carbonate content.

named K/C, the (002) peak of kaolinite on the (001) peak of illite (10 Å), named K/I, and the (002) peak of kaolinite on the (001) peak of *R0* I/S (~17 Å), named K/(I/S). The three large cyclic depletion/enrichment variations mentioned above are more visible using these ratios (Fig. 4). Short-term, high-amplitude variations in K/C, K/I and K/(I/S) ratios occur in the F-OAE interval (at a height of 2.5 to 5.5 m), while the carbonate content is not disturbed (Fig. 4).

Two non-parametric Wilcoxon signed-rank tests for paired samples were also computed for each clay mineral and clay mineral ratio, both for beds and underlying interbeds, and for beds and overlying interbeds. Marly interbeds are significantly enriched in kaolinite and illite, and present higher K/C, K/I and K/(I/S) ratios ($p<10^{-6}$), while I/S abundances are notably higher in limestones ($p<10^{-6}$). There is no significant difference in chlorite content between beds and interbeds ($p>0.72$).

5. Cyclostratigraphic results

The 2π-MTM analyses performed on the four proxies reveal significant broadband, rather than sharp, peaks (Fig. 5). This noisy spectrum is likely a consequence of sedimentation rate variations, which tend to broaden the peaks associated with a single frequency (Weedon, 2003).

Each clay mineral ratio displays a single, highly significant, broad peak (above the 99% confidence level), with maximum power for a period ranging from 16.7 to 10.4 m (Fig. 5A to C), while no significant peak is present at this position using carbonate content (Fig. 5D). The spectra of K/(I/S) and %$CaCO_3$ present two groups of peaks between 5 and 2 m, with differences between the proxies: significant peaks (above 95% confidence level) at 3.3 m for K/(I/S) (Fig. 5A), and at 3.7 and 2 m for %$CaCO_3$ (Fig. 5D). K/C and K/I ratios conversely show no significant peak in this band (Fig. 5B and C). A group of three peaks, at ca. 1.3, 1.0 and 0.7 m is identified for all proxies. The peak at 1.3 m is significant for K/(I/S) and %$CaCO_3$, the peak at 1.0 m is highly significant for all clay mineral ratios and significant for the %$CaCO_3$. The peak at 0.7 m is highly significant for %$CaCO_3$ and K/C, significant for K/(I/S) and non-significant for K/I. Between 0.6 and 0.5 m, all the spectra display two or three significant peaks.

An optimal solution appears by comparing the measured sedimentary period ratios to the theoretical Hauterivian period ratios. The peaks between 2 and 5 m are attributed to the short eccentricity

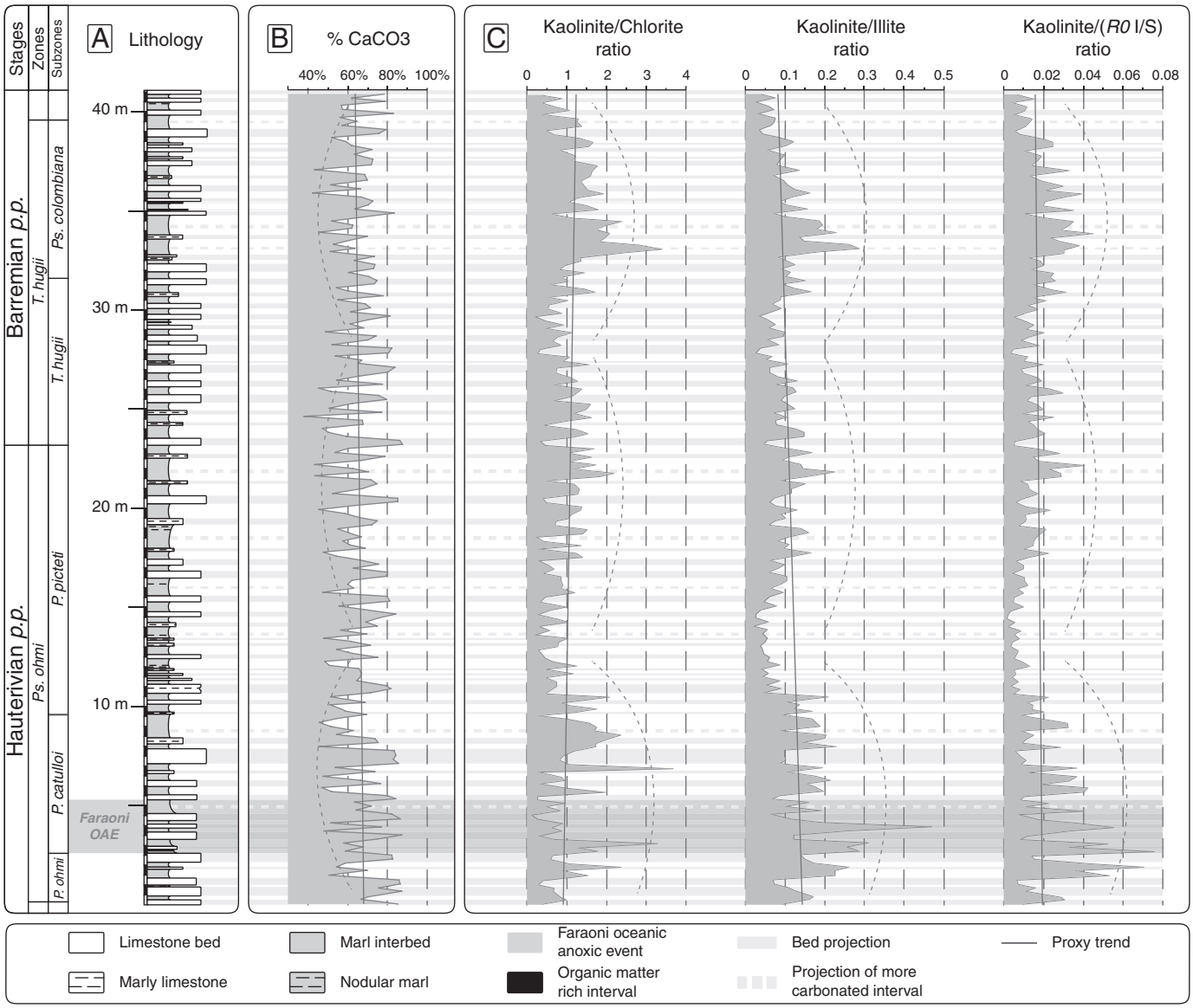

Fig. 4. Total carbonate content and variations of the clay mineral ratios used as climate proxies with their respective trends. The dotted lines highlight the cycles of increasing/decreasing values for the ratios.

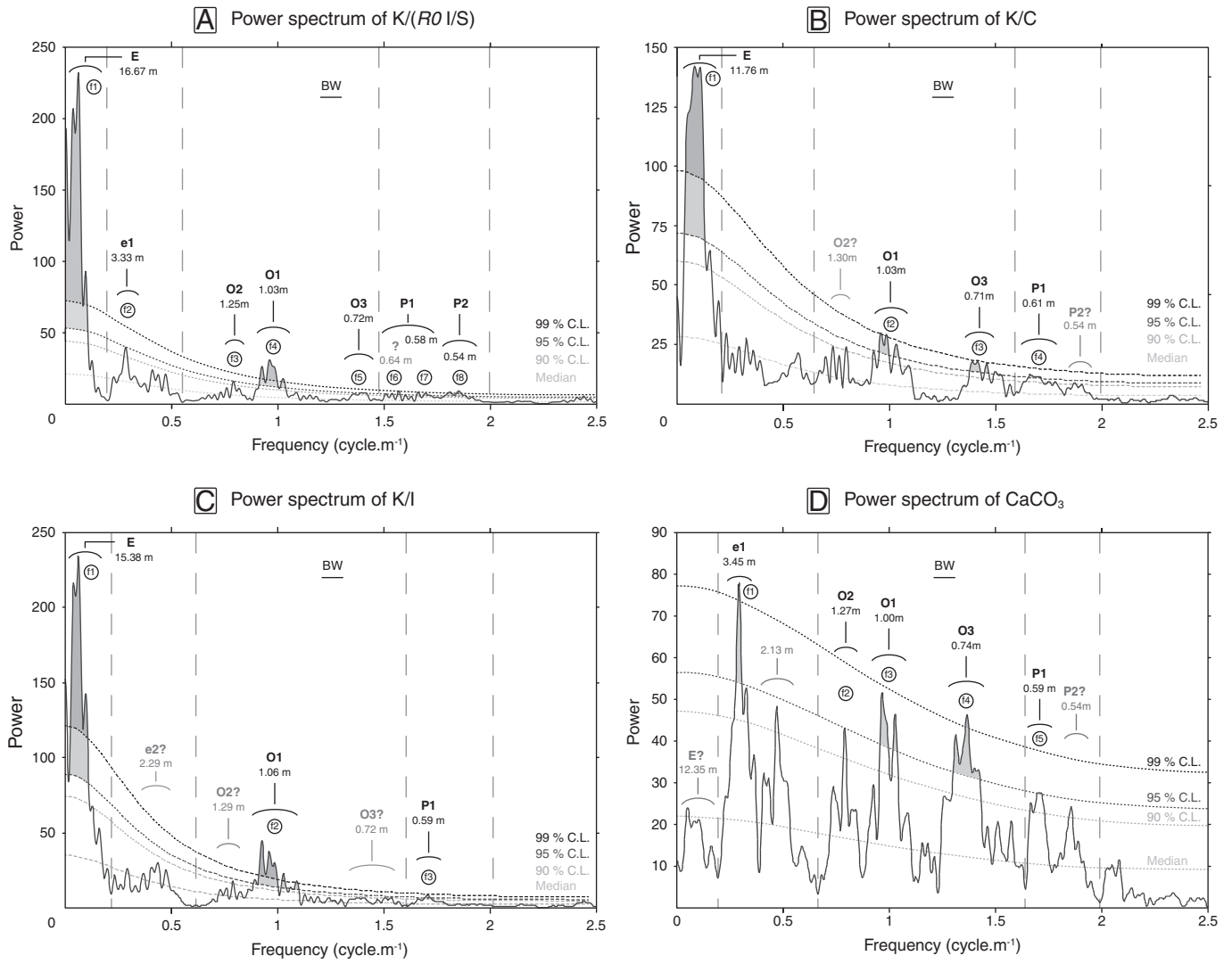

Fig. 5. 2π-MTM power spectra of (A) kaolinite/(*R0* I/S) ratio, (B) kaolinite/chlorite ratio, (C) kaolinite/ilite ratio and (D) carbonate calcium content. Median represents the red noise modelling smoothed at one-fifth of the Nyquist frequency. 90%, 95% and 99% confidence levels are also shown. The peaks up to 90% C.L. are used for the identification of the orbital cycles provided by the period ratios. Results are detailed for K/(*R0* I/S) in Table 1. Vertical dashed lines in the spectra separate 405 kyr-eccentricity, 100-kyr eccentricity, obliquity and precession bands. BW: bandwidth.

components (e1 and e2), the group of three peaks from 0.6 to 1.3 m corresponds to the three components of the obliquity (O2, O1 and O3), and the peaks between 0.5 and 0.6 m result from the components of the precession, P1 and P2. Concerning the first broad, highly significant peak, ratio values suggest the long eccentricity E, though the period is rather elevated for K/(I/S), leading to high sedimentary period ratios compared to the theoretical period ratios of E (Table 2). In the same section, similar periods were obtained using sediment magnetic susceptibility, with a better expression of the short eccentricity (Martinez et al., 2012).

The frequency bands of each proxy were isolated using Gaussian filters. For clay mineral ratios, three bands are tested for the eccentricity and one for the long precession (P1) cycle. Details are given for K/(I/S) in Fig. 6. The first band encompasses the short and long eccentricity, the second, only the short eccentricity, the third, only the long eccentricity (Fig. 7D), and the fourth, the long precession cycle (Fig. 7C). The filterings of the frequency band attributed to the short eccentricity and to P1 cycle display an amplitude modulation linked to the long eccentricity, as in astronomical solutions (Laskar et al., 2004; Fig. 7C and D). This supports our previous identifications of the eccentricity cycles on the sedimentary spectra. Three long eccentricity cycles (405 kyr) are identified throughout the series (Fig. 7D). On %$CaCO_3$, only the short eccentricity band was filtered due to the non-significance of the long eccentricity peak for this proxy (Fig. 5D). Thirteen short eccentricity cycles (100 kyr) are identified throughout the series for all the proxies.

Duration estimates are based on the filtering of the eccentricity from the different proxies. The assessed duration of the section is comprised from 1143 to 1229 kyr depending on the proxy selected, with an average of 1180 kyr, and an error margin estimated as 86 kyr, which corresponds to the greatest difference between the extreme values. This duration strongly differs from the 2250 kyr proposed in the GTS 2004 (Gradstein et al., 2004) and from the 550 kyr re-evaluated in the GTS 2008 (Ogg et al., 2008). The durations of the ammonite zones range from 570 to 702 kyr (average = 645 ± 28 kyr S.E.M.) for *P. ohmi* Zone and from 456 to 573 kyr (average = 535 ± 27 kyr S.E.M.) for *T. hugii* Zone (Table 2).

6. Discussion

6.1. Diagenetic influences

Smectite minerals are notoriously sensitive to temperature rise with burial depth, and completely disappear beyond 200 °C, after an exponential rate of illitisation between 120 °C and 150 °C (Nadeau

Table 1
(A) Comparison of period ratios from the power spectra of K/(*R0* I/S), and (B) theoretical Hauterivian orbital period ratios. Periods for which there is no correspondence with sedimentary periods are in grey. (C) Identification of the orbital cycles. Periods for which there is no correspondence with orbital periods are in grey.

A) Sedimentary period ratios of K/IS Periods	f1	f2	f3	f4	f5	f6	f7	f8
f1	1.000							
f2	0.200	1.000						
f3	0.075	0.375	1.000					
f4	0.062	0.309	0.825	1.000				
f5	0.043	0.217	0.580	0.703	1.000			
f6	0.038	0.191	0.510	0.618	0.879	1.000		
f7	0.035	0.175	0.468	0.567	0.807	0.918	1.000	
f8	0.032	0.162	0.432	0.524	0.746	0.849	0.924	1.000

B) Hauterivian orbital period ratios Paramet	E	e1	e2	O2	O1	O3	P1	P1
E	1.000							
e1	0.306	1.000						
e2	0.235	0.766	1.000					
O2	0.114	0.372	0.485	1.000				
O1	0.090	0.294	0.384	0.792	1.000			
O3	0.066	0.217	0.283	0.584	0.737	1.000		
P1	0.054	0.175	0.228	0.471	0.595	0.807	1.000	
P2	0.045	0.146	0.191	0.393	0.496	0.673	0.834	1.000

C) Orbital cycle identification Parameters (kyr)	Periods (m)
E (405)	f1 (16.67)
e1 (124)	f2 (3.33)
O2 (46.1)	f3 (1.25)
O1 (36.5)	f4 (1.03)
O3 (26.9)	f5 (0.72)
P1? (21.7)	f6 (0.64)
P1 (21.7)	f7 (0.58)
P2 (18.1)	f8 (0.54)

Table 2
Synthesis of the ammonite biozone durations proposed in this study, compared with the GTS2004 and GTS2008, and other cyclostratigraphic works.

Zone	Subzone	Height (m)	This study					Gradstein et al. (2004)	Ogg et al. (2008)	Fiet and Gorin (2000)	Bodin et al. (2006)	Sprovieri et al. (2006)	Martinez et al. (2012)
			%$CaCO_3$ (kyr)	K/C (kyr)	K/I (kyr)	K/(I/S) (kyr)	Average duration with standard error (kyr)						
P. ohmi	*P. ohmi*	0–2.6	72	73	69	61	69±3	650					
	P. catulloi	2.6–9.6	203	202	191	169	191±8	600					
	P. picteti	9.6–23.2	427	395	377	340	385±18	650					
	Total		702	670	637	570	645±28	1900	200	Not zoned	500	Not zoned	780
T. hugii	*T. hugii*	23.2–31.6	213	283	269	278	261±32						
	Ps. colombiana	31.6–39.6	243	276	283	295	274±11						
	Total		456	559	552	573	535±27	350	350	300	500	ca. 600	570
	Total		1158	1229	1189	1143	1180±19	2250	550	No data	1000		1350

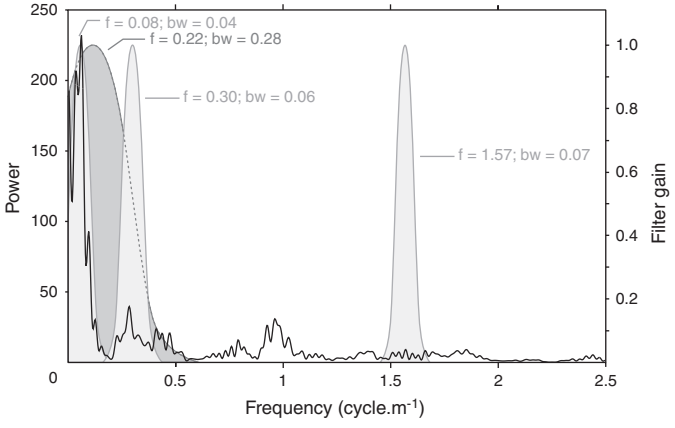

Fig. 6. Filtering of the power spectrum of K/(I/S), for the frequencies of the total eccentricity band (E + e1), the short eccentricity (e1), the long eccentricity (E), and the long precession (P1). The use of Gaussian filters (with "f" the mean frequency and "bw" the bandwidth) allows a progressive gain on the selected frequency band.

and Bain, 1986; Kübler and Jaboyedoff, 2000; Lanson et al., 2009; Środoń et al., 2009). The abundance of smectite sheets in *R0* I/S mixed layers (>50% of smectite sheets), which dominate the clay assemblages, indicate a weak burial diagenesis (Fig. 3). In addition, several elements show that diagenetic influence was very limited:

(i) The clay fraction in the limestone beds contains no chlorite-smectite mixed-layers or iron-rich chlorite, whose presence in coeval marl–limestone alternations from the Vocontian Basin indicates a diagenetic influence (Deconinck and Debrabant, 1985; Deconinck, 1987).
(ii) Basal reflections of kaolinite on diffractograms display broad peaks, implying disordered crystal structure, and thus a dominant detrital origin.
(iii) Organic matter from black shales of the Faraoni event is immature, with a T_{max} of 420 °C compatible with the presence of *R0* I/S (Dellisanti et al., 2010).

It is therefore reasonable to state that diagenetic effects on clay minerals are very limited in the section.

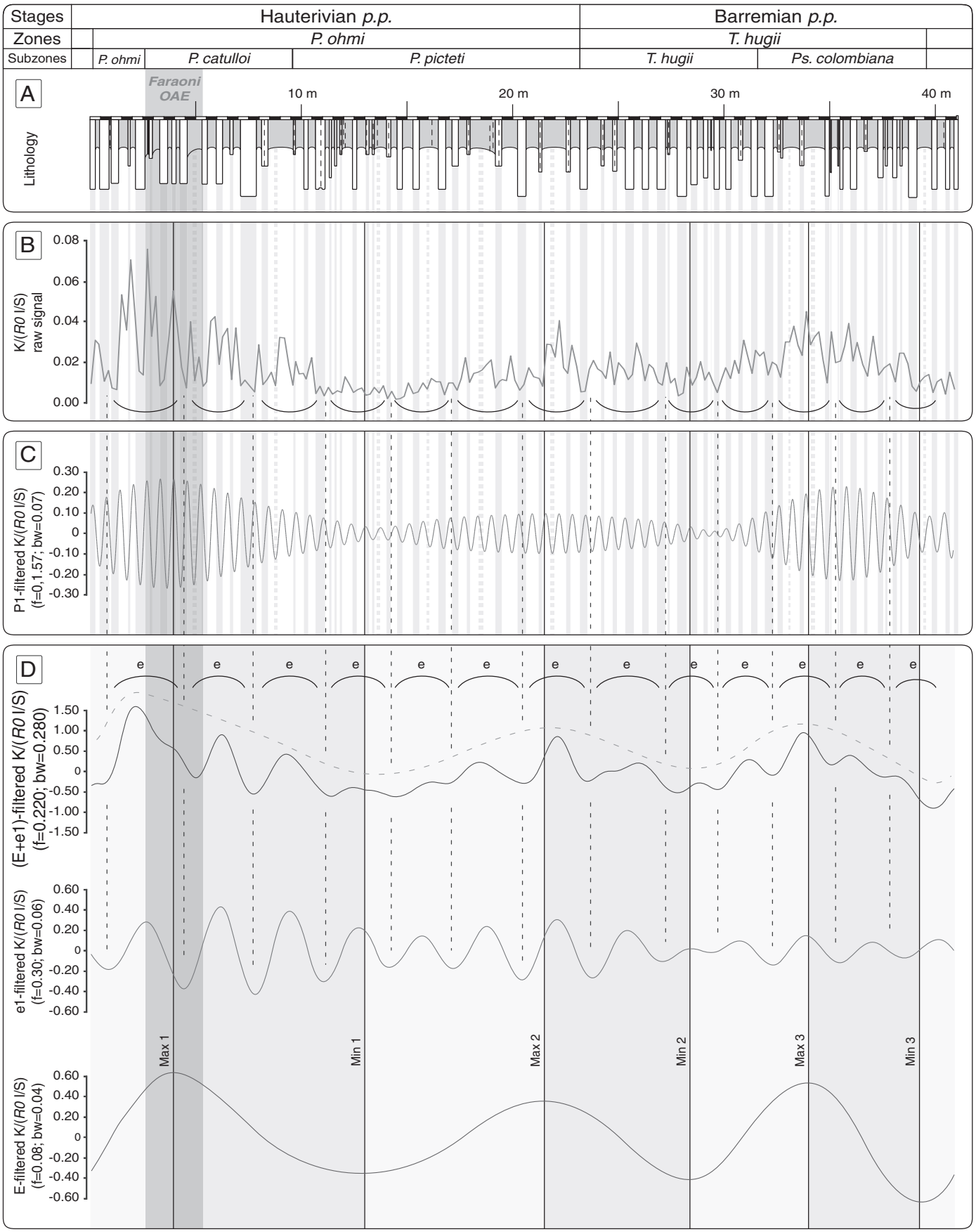

Fig. 7. Orbital calibration of K/(I/S). (A) Lithology of the X.Ag-1 section. (B) Variations of K/(*R0* I/S) raw signal. (C) P1-filtered signal, displaying the relation between one bed–interbed couplet and one cycle of the precession. (D) Filtering of K/(I/S) using the whole eccentricity band (E + e1), the short eccentricity band (e1 component) and the long eccentricity band (E).

Chlorite and illite are thought to be primary inherited minerals from the erosion of metamorphosed basement rocks from the adjacent Iberian massif, located north of the studied area (Fig. 1), and subsequently exported to the basins of the Subbetic Zone (Martín-Algarra et al., 1992; Barbero and López-Garrido, 2006), whereas kaolinite and I/S are probably reworked from palaeoalteration or contemporaneous soils. Consequently the clay assemblages in the Río Argos section are considered as dominantly composed of detrital minerals, whose composition is driven by climate and runoff variations on land.

Possible diagenetic artifacts can generate, or at least disturb, marl–limestone alternations, in which case, clay mineral assemblages display no variations in phase with lithological alternations (Westphal et al., 2010). In our study, systematic variations in primary clay mineral assemblages, in agreement with lithological changes, validate a genuine distribution of calcium carbonate in the Río Argos section, supporting a very limited diagenetic influence. The $CaCO_3$ content therefore results from biological productivity diluted by detrital supplies, largely dependent on climate conditions. The $CaCO_3$ content and the clay mineral ratios are therefore reliable palaeoclimate proxies in this section.

6.2. High-frequency clay mineralogical variations and orbital forcing

Clay minerals display a rhythmic response linked to the alternating lithology, with limestone beds systematically enriched in I/S mixed-layers, whereas marl interbeds are enriched in kaolinite and illite. The presence of kaolinite and illite in the clay mineral assemblages is interpreted as the result of high runoff under humid tropical conditions, whereas I/S mixed-layers were formed under seasonally contrasted semi-arid conditions (Deconinck and Chamley, 1983; Mutterlose and Ruffell, 1999). These distinct assemblages suggest a climate control on lithological alternations evolving from semi-arid conditions recorded in limestone beds, to tropical humid conditions recorded in marly interbeds.

The detection of orbital parameter characteristics in clay mineral ratios suggests an orbital control on clay mineral assemblages through the modification of climate conditions, mainly humidity. Spectral analyses of clay minerals show a significant band ranging from 0.6 to 0.7 m linked to the precession, also perceived in the $\%CaCO_3$ spectrum. This feature suggests a fundamental control of the precession on the marl–limestone alternations of the Río Argos section, recorded in the clay mineral assemblages. As showed in Fig. 7C, the P1-filtering of the K/(I/S) signal displays very close co-variations with marl–limestone couplets, and an amplitude modulation by the long precession oscillations as predicted by astronomical models (Laskar et al., 2004). Conversely to other views (Thiry, 2000), this example shows that clay minerals deposited in marine environments may record high-frequency climate fluctuations.

6.3. Comparisons with other duration estimates

Previous cyclostratigraphic duration estimates were based on cycle counting in the Vocontian Basin (Southeastern France; Huang et al., 1993; Giraud, 1995; Bodin et al., 2006) and in the Umbria–Marche Basin (Central Italy; Fiet and Gorin, 2000). An orbital calibration of the Maiolica Formation (Umbria–Marche Basin) based on the $\delta^{13}C$ is also provided by Sprovieri et al. (2006), despite large uncertainties of ammonite biozonation.

Based on the digitalised lithology processed for time-series analysis, Huang et al. (1993) identified the obliquity as the main driver of Hauterivian marl–limestone alternations in the Vocontian Basin. Giraud (1995) analysed a calcium carbonate curve digitalised accordingly to the lithology and suggested that the precession cycle was the main driver of marl–limestone alternations. Based on high-resolution calcium carbonate content measurements, Barremian marl–limestone alternations of Central Italy were attributed to precession cycles (Fiet and Gorin, 2000). Following the conclusions of Giraud (1995) and Fiet and Gorin (2000), cycle counting provided duration estimates of 500 kyr for each ammonite *P. ohmi* and *T. hugii* zones (Bodin et al., 2006). Compared to our assessments, these results are slightly lower for the *P. ohmi* Zone and in good agreement for the *T. hugii* Zone (Table 2). In Central Italy cycle counting provided an estimated duration of 300 kyr for the *T. hugii* Zone while this time interval was assessed at ca. 600 kyr by applying an orbital calibration on the $\delta^{13}C$ curve obtained for the Maiolica Formation (Sprovieri et al., 2006). This latter estimate is consistent with our assessment. No duration estimate can be deduced for the *P. ohmi* Zone since the boundaries are not established in this basin. Using the identification of the 100-kyr eccentricity on magnetic susceptibility in the Río Argos section, close estimated durations of 780 kyr for the *P. ohmi* Zone and 540 kyr for the *T. hugii* Zone have been recently proposed (Martinez et al., 2012). Durations of ammonite zones estimated in this study are in the same range as most reliable cyclostratigraphic studies performed in several basins of the Western Tethys, strengthening the reliability of our tuning. Our assessments differ from the GTS2004 and GTS2008, which are based on constant spreading rate of the Hawaiian seafloor and on fairly linear trend of Sr-isotope ratios curve for the Hauterivian (Ogg and Smith, 2004; McArthur et al., 2007).

6.4. Influence of the Faraoni event on orbital cycle records in the sediments

A short duration of the F-OAE is deduced from the orbital calibration since it encompasses approximately one oscillation of the short eccentricity (~100 kyr; Fig. 7D). This short-lived event is in good agreement with previous cyclostratigraphic results (Baudin, 2005), and coincides with disturbances in the clay mineral assemblages. Highest values of kaolinite and chlorite observed during the F-OAE (Fig. 3) likely result from the accelerated hydrological cycle, increasing nutrient supply and organic carbon storage in the sediments (Baudin, 2005; Godet et al., 2006; Bodin et al., 2009). This event is also expressed in the K/(I/S) fluctuations (Fig. 7B), which shows the highest values inducing disturbances in the eccentricity record. The consequence is an asymmetric shape of the first 405-kyr cycle observed in the series (Fig. 7D). The change in the sedimentary expression of orbital cycles induced by palaeoceanographic events challenges the hypothesis of OAE triggered by long-term orbital cycles (Mitchell et al., 2008).

7. Conclusions

This study reveals that clay minerals are reliable proxies to record high-frequency climate fluctuations triggered by orbital forcing at several scales, including precession, obliquity, and eccentricity:

(i) Lower Cretaceous marl–limestone alternations exposed on the Río Argos section are not substantially modified by diagenesis, preventing the primary detrital minerals from being transformed. As in the coeval marl–limestone alternations of the Vocontian Basin, the constitution of clay mineral assemblages is clearly different between limestone beds and marly interbeds. This relationship indicates regular climate oscillations. Higher contents of illite and kaolinite in marly interbeds suggest more humid conditions and increased runoff on the landmasses during the deposition of the interbeds. Conversely, the abundance of I/S mixed-layers in the clay fraction of the limestone beds is indicative of more arid climate conditions.

(ii) Spectral analyses performed on clay mineral ratios and $\%CaCO_3$ reveal frequency bands, which match orbital parameters. Subsequent filtering demonstrates the fundamental control of the precession on the deposit of one bed–interbed couplet, conveying the idea of a close relationship between orbital forcing on the climate and the export of clay minerals. This implies high

sensitivity of the sedimentary record of Río Argos and the short time response of detrital clay minerals to climate forcing. The 405 kyr-eccentricity band is particularly significant, allowing orbital calibration and duration estimates of ammonite zones. The average durations of the ammonite zones encompassing the section are estimated as 645 kyr for *P. ohmi* Zone and 535 kyr for *T. hugii* Zone.

(iii) The sedimentary expression of the orbital cycles is disturbed during the brief F-OAE, (ca. 100 kyr), suggesting an additional climatic control overprinting the orbital forcing.

Acknowledgements

Funding for this research was provided by the ANR project "Astronomical Time Scale for the Mesozoic and Cenozoic era". The authors gratefully thank Carmela Chateau-Smith (University of Burgundy) for English proof reading. Dr Béla Raucsik and an anonymous reviewer are acknowledged for their helpful and constructive reviews.

References

Aguado, R., Company, M., Tavera, J.M., 2000. The Berriasian/Valanginian boundary in the Mediterranean region: new data from the Caravaca and Cehegín sections, SE Spain. Cretaceous Research 21 (1), 1–21.

Barbero, L., López-Garrido, A.C., 2006. Mesozoic thermal history of the Prebetic continental margin (southern Spain): constraints from apatite fission-track analysis. Tectonophysics 422 (1–4), 115–128.

Barron, E.J., 1983. A warm, equable Cretaceous: the nature of the problem. Earth-Sciences Reviews 19 (4), 305–338.

Baudin, F., 2005. A Late Hauterivian short-lived anoxic event in the Mediterranean Tethys: the 'Faraoni event'. Comptes Rendus Geoscience 337 (16), 1532–1540.

Baudin, F., Busnardo, R., Beltran, C., de Rafélis, M., Renard, M., Charollais, J., Clavel, B., 2006. Enregistrement de l'événement anoxique Faraoni (Hauterivien supérieur) dans le domaine ultrahelvétique. Revue de Paléobiologie 25 (2), 525–535.

Berger, A., Loutre, M.F., 2004. Théorie astronomique des paléoclimats. Comptes Rendus Geoscience 336 (7–8), 701–709.

Bodin, S., Godet, A., Föllmi, K.B., Vermeulen, J., Arnaud, H., Strasser, A., Fiet, N., Adatte, T., 2006. The late Hauterivian Faraoni oceanic anoxic event in the western Tethys: evidence from phosphorus burial rates. Palaeogeography Palaeoclimatology Palaeoecology 235, 245–264.

Bodin, S., Fiet, N., Godet, A., Matera, V., Westermann, S., Clement, A., Janssen, N.M.M., Stille, P., Föllmi, K.B., 2009. Early Cretaceous (late Berriasian to Early Aptian) palaeoceanographic change along the northwestern Tethyan margin (Vocontian Trough, southeastern France): $\delta^{13}C$, $\delta^{18}O$ and Sr-isotope belemnite and whole-rock records. Cretaceous Research 30 (5), 1247–1262.

Boulila, S., Galbrun, B., Hinnov, L.A., Collin, P.Y., 2008. High-resolution cyclostratigraphic analysis from magnetic susceptibility in a Lower Kimmeridgian (Upper Jurassic) marl–limestone succession (La Méouge, Vocontian Basin, France). Sedimentary Geology 203 (1–2), 54–63.

Boulila, S., de Rafélis, M., Hinnov, L.A., Gardin, S., Galbrun, B., Collin, P.-Y., 2010a. Orbitally forced climate and sea-level changes in the Paleoceanic Tethyan domain (marl–limestone alternations, Lower Kimmeridgian, SE France). Palaeogeography, Palaeoclimatology, Palaeoecology 292 (1–2), 57–70.

Boulila, S., Galbrun, B., Hinnov, L.A., Collin, P.-Y., Ogg, J.G., Fortwengler, D., Marchand, D., 2010b. Milankovitch and sub-Milankovitch forcing of the Oxfordian (Late Jurassic) Terres Noires Formation (SE France) and global implications. Basin Research 22 (5), 717–732.

Chamley, H., 1989. Clay Sedimentology. Springer-Verlag, Berlin . (623 pp.).

Company, M., 1987. Los Ammonites del Valanginiense del sector oriental de las Cordilleras Béticas (SE de España). PhD thesis, University of Grenada, 294 p.

Company, M., Sandoval, J., Tavera, J.M., 1995. Lower Barremian ammonite biostratigraphy in the Subbetic Domain (Betic Cordillera, southern Spain). Cretaceous Research 16 (2–3), 243–256.

Company, M., Sandoval, J., Tavera, J.M., 2003. Ammonite biostratigraphy of the uppermost Hauterivian in the Betic Cordillera (SE Spain). Geobios 36 (6), 685–694.

Cotillon, P., Giraud, F., 1995. Comparative evolution of material flux through two DSDP successions from Central Atlantic and Gulf of Mexico. Preliminary results of a new approach to sedimentary dynamics in pelagic environments. Marine Geology 122 (4), 329–348.

Cotillon, P., Ferry, S., Gaillard, C., Jautée, E., Latreille, G., Rio, M., 1980. Fluctuation des paramètres du milieu marin dans le domaine vocontien (France Sud-Est) au Crétacé inférieur: mise en évidence par l'étude des formations marno-calcaires alternantes. Bulletin de la Société Géologique de France 5, 735–744.

Darmedru, C., 1984. Variations du taux de sédimentation et oscillations climatiques lors du dépôt des alternances marne-calcaire pélagiques. Exemple du Valanginien supérieur vocontien (Sud-Est de la France). Bulletin de la Société Géologique de France 1, 63–70.

Deconinck, J.-F., 1987. Identification de l'origine détritique ou diagénétique des assemblages argileux: le cas des alternances marne-calcaire du Crétacé inférieur subalpin. Bulletin de la Société Géologique de France 1, 139–145.

Deconinck, J.-F., 1992. Clay mineralogy of Early Cretaceous sediments of South-East France: Berriasian stratotype, Berriasian and Barremian of angles. Sequence Stratigraphy of European Basins, Dijon, Abstract Volume, pp. 366–367.

Deconinck, J.-F., Chamley, H., 1983. Héritage et diagenèse des minéraux argileux dans les alternances marno-calcaires du Crétacé inférieur du domaine subalpin. Comptes rendus de l'Académie des sciences 297 (7), 589–594.

Deconinck, J.-F., Debrabant, P., 1985. La diagenèse des argiles dans la domaine subalpin: rôles respectifs de la lithologie, de l'enfouissement, et de la surcharge tectonique. Revue de Géographie Physique et de Géologie Dynamique 26 (5), 321–330.

Dellisanti, F., Pini, G.A., Baudin, F., 2010. Use of Tmax as a thermal maturity indicator in orogenic successions and comparison with clay mineral evolution. Clay minerals 45, 115–130.

Fiet, N., Gorin, G., 2000. Lithologic expression of Milankovitch cyclicity in carbonate-dominated, pelagic, Barremian deposits in central Italy. Cretaceous Research 21 (4), 457–467.

Foucault, A., Mélières, F., 2000. Palaeoclimatic cyclicity in central Mediterranean Pliocene sediments: the mineralogical signal. Palaeogeography, Palaeoclimatology, Palaeoecology 158 (3–4), 311–323.

Gale, A.S., Bown, P., Caron, M., Crampton, J., Crowhurst, S.J., Kennedy, W.J., Petrizzo, M.R., Wray, D.S., 2011. The uppermost Middle and Upper Albian succession at the Col de Palluel, Haute-Alpes France: an integrated study (ammonites, inoceramid bivalves, planktonic foraminifera, nannofossils, geochemistry, stable oxygen and carbon isotopes, cyclostratigraphy). Cretaceous Research 32 (2), 59–130.

Ghil, M., Allen, M.R., Dettinger, M.D., Ide, K., Kondrashov, D., Mann, M.E., Robertson, A.W., Saunders, A., Tian, Y., Varadi, F., Yiou, P., 2002. Advanced spectral methods for climatic time series. Reviews of Geophysics 40 (1), 3.1-3.41.

Giraud, F., 1995. Recherche des périodicités astronomiques et des fluctuations du niveau marin à partir de l'étude du signal carbonaté des séries pélagiques alternantes. Documents des Laboratoires de Géologie de Lyon, No. 134. Centre des sciences de la terre, Université Claude-Bernard, Lyon, 279 pp.

Godet, A., Bodin, S., Föllmi, K.B., Vermeulen, J., Gardin, S., Fiet, N., Adatte, T., Berner, Z., Stüben, D., van de Schootbrugge, B., 2006. Evolution of the marine stable carbon-isotope record during the Early Cretaceous: a focus on the late Hauterivian and Barremian in the Tethyan realm. Earth and Planetary Science Letters 242 (3–4), 254–271.

Godet, A., Bodin, S., Adatte, T., Föllmi, K.B., 2008. Platform-induced clay-mineral fractionation along a northern Tethyan basin-platform transect: implications for the interpretation of Early Cretaceous climate change (Late Hauterivian–Early Aptian). Cretaceous Research 29 (5–6), 830–847.

Gradstein, F.M., Ogg, J.G., Smith, A.G., 2004. A Geologic Time Scale 2004. Cambridge University Press, Cambridge . (610 pp.).

Grippo, A., Fischer, A.G., Hinnov, L.A., Herbert, T.D., Premoli Silva, I., 2004. Cyclostratigraphy and chronology of the Albian stage (Piobbico core, Italy). In: D'Argenio, B., Fischer, A.G., Premoli Silva, I., Weissert, H., Ferreri, V. (Eds.), Cyclostratigraphy: Approaches and Case Histories. : SEPM Special Publication, No. 81. SEPM (Society for Sedimentary Geology), Tulsa, pp. 57–81.

Hallam, A., 1985. A review of Mesozoic climates. Journal of the Geological Society of London 142, 433–445.

Herbert, T.D., 1992. Paleomagnetic calibration of Milankovitch cyclicity in Lower Cretaceous sediments. Earth and Planetary Science Letters 112 (1–4), 15–28.

Hilgen, F.J., Kuiper, K.F., Lourens, L.J., 2010. Evaluation of the astronomical time scale for the Paleocene and earliest Eocene. Earth and Planetary Science Letters 300 (1–2), 139–151.

Hinnov, L.A., Ogg, J.G., 2007. Cyclostratigraphy and the astronomical time scale. Stratigraphy 4 (2–3), 239–251.

Hoedemaeker, P.J., 1998. A Tethyan–Boreal correlation of pre-Aptian Cretaceous strata: correlating the uncorrelatables. Geologica Carpathica 50 (2), 101–124.

Hoedemaeker, P.J., Leereveld, H., 1995. Biostratigraphy and sequence stratigraphy of the Berriasian–lowest Aptian (Lower Cretaceous) of the Río Argos succession, Caravaca, SE Spain. Cretaceous Research 16 (2–3), 195–230.

Huang, Z., Ogg, J.G., Gradstein, F.M., 1993. A quantitative study of Lower Cretaceous cyclic sequences from the Atlantic Ocean and the Vocontian Basin (SE France). Paleoceanography 8 (2), 275–291.

Huang, C.J., Hinnov, L., Fischer, A.G., Grippo, A., Herbert, T., 2010. Astronomical tuning of the Aptian Stage from Italian reference section. Geology 38 (10), 899–902.

Husson, D., Galbrun, B., Laskar, J., Hinnov, L.A., Thibault, N., Gardin, S., Locklair, R.E., 2011. Astronomical calibration of the Maastrichtian (Late Cretaceous). Earth and Planetary Sciences Letters 305 (3–4), 328–340.

Inoue, A., Bouchet, A., Velde, B., Meunier, A., 1989. Convenient technique for estimating smectite layer percentage in randomly interstratified illite/smectite minerals. Clays and Clay Minerals 37 (3), 227–234.

Kübler, B., Jaboyedoff, M., 2000. Illite crystallinity: concise review paper. Comptes Rendus de l'Académie des Sciences série II Fascicule A-Sciences de la Terre et des Planètes 331 (2), 75–89.

Lamas, F., Irigaray, C., Oteo, C., Chacón, J., 2005. Selection of the most appropriate method to determine the carbonate content for engineering purposes with particular regard to marls. Engineering Geology 81 (1), 32–41.

Lanson, B., Sakharov, B.A., Claret, F., Drits, V.A., 2009. Diagenetic smectite-to-illite transition in clay-rich sediments: a reappraisal of X-ray diffraction results using the multi-specimen method. American Journal of Science 309 (6), 476–516.

Laskar, J., Robutel, P., Joutel, F., Gastineau, M., Correia, A.C.M., Levrard, B., 2004. A long-term numerical solution for the insolation quantities of the Earth. Astronomy and Astrophysics 428 (1), 261–285.

Laskar, J., Fienga, A., Gastineau, M., Manche, H., 2011. La2010: a new orbital solution for the long-term motion of the Earth. Astronomy and Astrophysics 532 (A89) (15 pp.).
Lourens, L.J., Hilgen, F.J., Laskar, J., Shackleton, N.J., Wilson, D., 2004. The Neogene period. In: Gradstein, F.M., Ogg, J.G., Smith, A.G. (Eds.), A Geologic Time Scale 2004. Cambridge University Press, Cambridge, pp. 409–440.
Mann, M.E., Lees, J., 1996. Robust estimation of background noise and signal detection in climatic time series. Climatic Change 33 (3), 409–445.
Martín-Algarra, A., Ruiz-Ortiz, P.A., Vera, J.A., 1992. Factors controlling Cretaceous turbidite deposition in the Betic Cordillera. Revista de la Sociedad Geológica de España 5, 53–80.
Martinez, M., Pellenard, P., Deconinck, J.-F., Monna, F., Riquier, L., Boulila, S., Moiroud, M., Company, M., 2012. An orbital floating time scale of the Hauterivian/Barremian GSSP from a magnetic susceptibility signal (Río Argos, Spain). Cretaceous Research 36, 106–115.
Masse, J.-P., Bellion, Y., Benkhelil, J., Boulin, J., Cornee, J.J., Dercourt, J., Guiraud, R., Mascle, G., Poisson, A., Ricou, L.E., Sandulescu, M., 1993. Lower Aptian palaeoenvironments (114 to 112 Ma). In: Dercourt, J., Ricou, L.E., Vrielynck, B. (Eds.), Atlas Tethys Palaeoenvironmental Maps, BEICIP-FRANLAB. Gauthier-Villars, Reuil-Malmaison, Paris, pp. 135–152.
McArthur, J.M., Janssen, N.M.M., Reboulet, S., Leng, M.J., Thirwall, M.F., van de Schootbrugge, B., 2007. Palaeotemperatures, polar ice-volume, and isotope stratigraphy (Mg/Ca, $\delta^{18}O$, $\delta^{13}C$, $^{87}Sr/^{86}Sr$): the Early Cretaceous (Berriasian, Valanginian, Hauterivian). Palaeogeography, Palaeoclimatology, Palaeoecology 248 (3–4), 391–430.
Meyers, S.R., Sageman, B.B., 2004. Detection, quantification, and significance of hiatuses in pelagic and hemipelagic strata. Earth and Planetary Science Letters 224 (1–2), 55–72.
Milankovitch, M., 1941. Kanon der Erdbestrahlung und seine Anwendung auf das Eiszeitenproblem. Royal Serbian Academy Special Publication 132. section of Mathematical and natural Sciences, vol. 33. Belgrade (633 pp.).
Mitchell, R.N., Bice, D.M., Montanari, A., Cleaveland, L.C., Christianson, K.T., Coccioni, R., Hinnov, L.A., 2008. Oceanic anoxic cycles? Orbital prelude to Bonarelli Level (OAE 2). Earth and Planetary Science Letters 267, 1–16.
Moore, D.M., Reynolds, R.C., 1997. X-Ray Diffraction and the Identification and Analysis of Clay Minerals, 2nd edition. Oxford University Press, Inc., New York, NY . (400 pp.).
Munnecke, A., Westphal, H., Elrick, M., Reijmer, J.J.G., 2001. The mineralogical composition of precursor sediments of calcareous rhythmites: a new approach. International Journal of Earth Sciences 90, 795–812.
Mutterlose, J., Ruffell, A.H., 1999. Milankovitch-scale palaeoclimate changes in pale-dark bedding rhythms from the Early Cretaceous (Hauterivian and Barremian) of eastern England and northern Germany. Palaeogeography, Palaeoclimatology, Palaeoecology 154 (3), 133–160.
Nadeau, P.H., Bain, D.C., 1986. Composition of some smectites and diagenetic illitic clays and implications for their origin. Clays and Clay Minerals 34 (4), 455–464.
Ogg, J.G., Smith, A.G., 2004. The geomagnetic polarity time scale. In: Gradstein, F.M., Ogg, J.G., Smith, A.G. (Eds.), A Geologic Time Scale 2004. Cambridge University Press, Cambridge, pp. 63–86.
Ogg, J.G., Ogg, G., Gradstein, F.M., 2008. A Concise Geologic Time Scale 2008. Cambridge University Press, Cambridge . (184 pp.).
Paillard, D., Labeyrie, L., Yiou, P., 1996. Macintosh program performs time-series analysis. EOS, Transactions of the American Geophysical Union 77 (39), 379.
Petschick, R., 2000. (MacDiff 4.2.5 [Online]. Available:) http://servermac.geologie.uni-frankfurt.de/Rainer.html.
Price, G.D., 1999. The evidence and implications of polar ice during the Mesozoic. Earth-Science Reviews 48 (3), 183–210.
Pucéat, E., Lécuyer, C., Sheppard, S.M.F., Dromart, G., Reboulet, S., Grandjean, P., 2003. Thermal evolution of Cretaceous Tethyan marine waters inferred from oxygen isotope composition of fish tooth enamels. Paleoceanography 18 (2), 7.1-7.12.
Rasplus, L., Fourcade, E., Ambroise, D., Andeol, B., Azéma, J., Blanc, P., Busnardo, R., Clerc-Renaud, T., Damotte, R., Dercourt, J., Foucault, A., Galbrun, B., Granier, B., Lachkar, G., Le Hégarat, G., Magné, J., Manivit, H., Mangin, A.-M., Masure, E., Mazaud, A., Michaud, F., Morand, F., Renard, M., Schuber, N., Taugourdeau, J., 1987. Stratigraphie intégrée du sillon citrabétique (Sierra de Fontcalent, Province d'Alicante, Espagne). Geobios 20 (3), 337–387.
Rio, M., Cotillon, P., Ferry, S., 1989. Périodicités dans les séries pélagiques alternantes et variations de l'orbite terrestre. Exemple du Crétacé inférieur dans le Sud-Est de la France. Comptes rendus de l'Académie des Sciences - Série II 309 (1), 73–79.
Sprenger, A., Ten Kate, W.G., 1993. Orbital forcing of calcilutite marl cycle in Southeast Spain and an estimate for the duration of the Berriasian Stage. Geological Society of American Bulletin 105 (6), 807–818.
Sprovieri, M., Coccioni, R., Lirer, F., Pelosi, N., Lozar, F., 2006. Orbital tuning of a lower Cretaceous composite record (Maiolica Formation, central Italy). Paleoceanography 21, PA4212. http://dx.doi.org/10.1029/2005PA001224.
Środoń, J., Clauer, N., Huff, W., Dudek, T., Banaś, M., 2009. K–Ar dating of the Lower Palaeozoic K-bentonites from the Baltic Basin and the Baltic Shield: implications for the role of temperature and time in the illitization of smectite. Clay minerals 44, 361–387.
Strasser, A., Hilgen, F.J., Heckel, P.H., 2006. Cyclostratigraphy — concepts, definitions, and applications. Newsletters on Stratigraphy 42 (2), 75–114.
Thiry, M., 2000. Palaeoclimatic interpretation of clay minerals in the marine deposits: an outlook from the continental origin. Earth-Sciences Reviews 49 (1–4), 201–221.
Thomson, D.J., 1982. Spectrum estimation and harmonic analysis. Proceedings of the Institute of Electrical and Electronics Engineers 70 (9), 1055–1096.
Thomson, D.J., 1990. Time series analysis of Holocene climate data. Philosophical Transactions of the Royal Society of London A 330 (1615), 601–616.
van de Schootbrugge, B., Föllmi, K.B., Bulot, L.G., Burns, S.J., 2000. Paleoceanographic changes during the early Cretaceous (Valanginian–Hauterivian): evidence from oxygen and carbon stable isotopes. Earth and Planetary Science Letters 181 (1–2), 15–31.
Vanderaveroet, P., Averbuch, O., Deconinck, J.-F., Chamley, H., 1999. A record of glacial/interglacial alternations in Pleistocene sediments off New Jersey expressed by clay mineral, grain-size and magnetic susceptibility data. Marine Geology 159 (1–4), 79–92.
Voigt, S., Schönfeld, J., 2010. Cyclostratigraphy of the reference section for the Cretaceous white chalk of northern Germany, Lägerdorf–Kronsmoor: a late Campanian–early Maastrichtian orbital time scale. Palaeogeography, Palaeoclimatology, Palaeoecology 287 (1–4), 67–80.
Weedon, G.P., 2003. Time-Series Analysis and Cyclostratigraphy. Cambridge University Press, Cambridge . (259 pp.).
Westphal, H., Hilgen, F., Munnecke, A., 2010. An assessment of the suitability of individual rhythmic carbonate successions for astrochronological application. Earth-Science Reviews 99 (1–2), 19–30.